Photochemistry and Photobiology, 2006, 82: 733–737

Photoionization Thresholds of Melanins Obtained from Free Electron Laser–Photoelectron Emission Microscopy, Femtosecond Transient Absorption Spectroscopy and Electron Paramagnetic Resonance Measurements of Oxygen Photoconsumption

Tong Ye[1], Lian Hong[1], Jacob Garguilo[2], Anna Pawlak[3], Glenn S. Edwards[4], Robert J. Nemanich[2], Tadeusz Sarna[3] and John D. Simon*[1]

[1]Department of Chemistry, Duke University, Durham, NC
[2]Department of Physics, North Carolina State University, Raleigh, NC
[3]Department of Biophysics, Jagiellonian University, Krakow, Poland
[4]Department of Physics, Duke University, Durham, NC

Received 30 December 2005; accepted 13 March 2006; published online 16 March 2006 DOI: 10.1562/2006-01-02-RA-762

ABSTRACT

Free electron laser–photoelectron emission microscopy (FEL-PEEM), femtosecond absorption spectroscopy and electron paramagnetic resonance (EPR) measurements of oxygen photoconsumption were used to probe the threshold potential for ionization of eumelanosomes and pheomelanosomes isolated from human hair. FEL-PEEM data show that both pigments are characterized by an ionization threshold at 282 nm. However, pheomelanosomes exhibit a second ionization threshold at 326 nm, which is interpreted to be reflective of the benzothiazine structural motif present in pheomelanin and absent in eumelanin. The lower ionization threshold for pheomelanin is supported by femtosecond transient absorption spectroscopy. Unlike photolysis at 350 nm, following excitation of solubalized synthetic pheomelanin at 303 nm, the transient spectrum observed between 500 and 700 nm matches that for the solvated electron, indicating the photoionization threshold for the solubalized pigment is between 350 and 303 nm. For the same synthetic pheomelanin, EPR oximetry experiments reveal an increased rate of oxygen uptake between 338 nm and 323 nm, narrowing the threshold for photoionization to sit between these two wavelengths. These results on the solubalized synthetic pigment are consistent with the FEL-PEEM results on the human melanosomes. The lower ionization potential observed for pheomelanin could be an important part of the explanation for the greater incidence rate of UV-induced skin cancers in red-haired individuals.

INTRODUCTION

Epidemiological studies reveal that people with different pigments have varying risk factors for both nonmelanoma and melanoma skin cancers. Red-haired and blond-haired individuals have been assessed to have three to six times and 1.3 times higher risk, respectively, for developing nonmelanoma skin cancers than those with dark hair (1). In the case of melanoma, Veierød and coworkers found that the risk for red-hair individuals was four times higher than that for black- or dark brown-haired individuals (2).

Differences in natural hair color reflect the underlying molecular composition of the melanin pigment. Melanins are generally classified into two types: pheomelanin (the yellow-red pigment) and eumelanin (the brown-black pigment) (3,4). The two melanins share a common beginning to the melanogenesis pathway. Eumelanin derives from the oxidative oligomerization of tyrosine. The two central monomer units commonly invoked in the discussion of the eumelanin pigment are 5,6-dihydroxyindole and, 5,6-dihydroxyindole-2-carboxylic acid. For pheomelanin, the synthesis of leucodopachrome in the eumelanin pathway completes the reaction of dopaquinone and cysteine to form 5-S-cysteinyldopa, which then reacts to form benzothiazine moieties that are incorporated in the final pigment.

The hair and skin melanocytes share a common embryonic origin, both originating from the neural crest (5), so it is reasonable to hypothesize that they could make the same pigment. In a detailed study along these lines, Thody and coworkers studied the eumelanin and pheomelanin content present in the epidermis of varying skin types and compared those results with the corresponding content in hair (6). They found that the ratio of pheomelanin to eumelanin in the epidermis correlated with that in hair, but that the concentration of the pigment in hair was in excess of 20 times that in the epidermis. This study establishes that the pigment present in hair can be used as an excellent model for that present in the melanocyte in skin. The epidemiological data therefore suggest that an increased risk for melanoma and nonmelanoma skin cancers exists with higher pheomelanin content. Expanding on this idea, Prota and coworkers found a relationship between the skin's minimal erythemal dose and the pheomelanin-to-eumelanin ratio in the hair, indicating that UV sensitivity is associated with high pheomelanin and low eumelanin levels (7). However, recent work by Hennessy *et al.* examined eumelanin and pheomelanin concentrations in human skin before and after exposure to UV radiation (8). Their findings show little change in the ratio of these pigments between skin types or upon exposure to UV radiation, suggesting that the presence of pheomelanin (or the ratio of eumelanin to pheomelanin) does not

*Corresponding author email: jsimon@duke.edu (John D. Simon)

account for the difference in UV sensitivity between different skin types. They speculate that factors other than the amount of pheomelanin may be important in determining the susceptibility of persons with red hair to UV radiation.

The above discussion raises the question as to whether the relative risk factors are associated with the UV-photoreaction(s) of the different pigments. A suggestion in support of a causative role of pigments is that UV-A–induced single-strand DNA breaks in human melanocytes differing only in the amount of pigment produced showed photosensitization is induced by intrinsic chromophores, most likely pheomelanin and/or melanin intermediates (9). Further evidence was recently reported by Brash and coworkers who examined the induction of DNA lesions and apoptosis upon UV exposure of congenic mice of with black, yellow and albino coats (10). UV-B–induced cyclobutane dimerization and apoptosis measured by sunburn cells or keratinocytes containing active caspase-3 was strain independent. Combining the results of measurements on TUNEL-positive cells with the concentration of pigments in the different mice revealed that pheomelanin had a three-fold greater activity, establishing that pheomelanin sensitizes apoptosis (via caspase-3 activation) in adjacent cells at a frequency greater than that induced by direct DNA absorption.

This paper examines the role of pheomelanin sensitization based on an observation reported by Chedekel and coworkers in 1980 (11). In contrast to eumelanin, these researchers found that pheomelanin undergoes rapid photodecomposition in the presence of oxygen upon exposure to UV light (12,13). They proposed that the primary photochemical process is the photoionization of electrons followed by subsequent formation of the superoxide radical anion.

$$\text{Pheomelanin} + h\nu \rightarrow e_{aq}^- + \text{pheomelanin radical} \quad (1)$$

$$e_{aq}^- + O_2 \rightarrow O_2^{\bullet -} \quad (2)$$

Thus, photolysis of the pigment consumes oxygen by generating $O_2^{\bullet -}$; the quantum yield for this process was reported to be $\sim 7.1 \times 10^{-4}$ for excitation at 360 nm. In 2002, we reported the transient spectrum following photolysis of pheomelanin at 350 nm, which revealed no evidence for formation of e_{aq}^-, indicating that at this wavelength the photoionization quantum yield was less than 2×10^{-5} (14). In this paper we examine the photoionization of pheomelanin using three complementary experimental approaches, free-electron laser–photoelectron emission microscopy (FEL-PEEM) (15,16), ultrafast transient absorption spectroscopy and oxygen photoconsumption as measured by electron paramagnetic resonance (EPR). The FEL-PEEM measurements are made on intact human melanosomes under vacuum. The transient absorption and EPR experiments are reported on synthetic pigments in aqueous solutions. Taken together, the three approaches establish that photoionization of pheomelanin occurs for wavelengths shorter than ~330 nm, in the UV-A region of the spectrum. Eumelanin, on the other hand, does not show this behavior, and its photoionization threshold is in the UV-B region (~280 nm).

MATERIALS AND METHODS

Melanosomes and pigments. Details of the isolation and characterization of the samples of human black- and red-hair melanosomes have been published before (17,18). The synthetic pigments were made as described previously (19).

Photoelectron emission microscopy. The details of the FEL-PEEM experiment have recently been reported (15). We utilized the spontaneous emission mode of the Duke UV-FEL in the spectral range of 207–344 nm (6.0–3.6 eV), with an energy full width at half maximum of ~0.1 eV. The PEEM images were acquired with a DVC 1312M digital camera from DVC Company, Inc., with a resolution of 1300 × 1030 pixels × 12 bits. The DVC View program was used to view and save images. We typically imaged assemblies of eumelanosomes at a field of views in the PEEM of 150 μm, and single eumelanosomes at a field of view of 5 or 1.5 μm. The focusing of the FEL was optimized for each wavelength used; the FEL spot size on the sample was ~30 × 100 μm. Samples were prepared as follows. Prior to deposition of melanosomes, (001) oriented silicon wafer sections were cleaned using an RCA wet chemical process, which left the surface terminated with a ~1 nm oxide layer. Films of melanosomes were prepared by spreading the suspension of melanosomes in nanopure water over the freshly cleaned wafers and allowing it to dry in air for less than 1 h.

The FEL-PEEM data was analyzed according to the theoretical model reported by Fowler (20). The intensity of the electron signal S depends on the temperature of the sample and is a function of the difference between the photon energy (hν) and the thermionic work function (X), $X = X_0 - \varepsilon^*$ where ε^* is the energy of the highest occupied molecular orbital and X_0 is the threshold potential, as given by (Eq. 3)

$$S(X_0 - h\nu)^{1/2} = AT^2 f[(h\nu - X)/k_B T] \quad (3)$$

where

$$f(u) = e^u - e^{2u}/2 - [e^{-u} - e^{-2u}/4 + e^{-3u}/9 - \ldots], \quad \text{for } (u \leq 0) \quad (4)$$

and

$$f(u) = \pi^2/6 + u^2/2 - [e^{-u} - e^{-2u}/4 + e^{-3u}/9 - \ldots], \quad \text{for } (u \geq 0) \quad (5)$$

Because of the presence of different functional groups in the pigment, it is possible to observe more than one threshold potential. Each such threshold would be described by the above functional form. Thus the threshold potential(s) can be determined by a nonlinear least-square fit of (Eq. 3), or a linear combination of the form given in (Eq. 3), of a plot of S/T^2 *vs* $h\nu/k_B T$.

Ultrafast spectroscopy. Experiments were conducted using a commercial regeneratively amplified Ti:Sapphire laser system (Spitfire, Spectra Physics, 120 fs [FWHM], 0.9 mJ/pulse centered at 800 nm, 1 kHz repetition rate) (21). Tunable light pulses were generated from the second harmonic of the output of an optical parametric amplifier (Spectra Physics, Mountain View, CA). The pump-probe transient absorption measurement setup was described previously in detail. The beam diameters of both the pump and probe at the region of spatial overlap within the sample were determined enabling quantitative analyses on observed signal intensities. Excitation wavelengths of 400 nm, 350 nm and 303 nm were used. The optical density of the sample at 527 nm was 1.0 OD in a 1 mm quartz cuvette ($\sim 10^{-3}$ *M*). All transient optical experiments were performed orienting the polarization of the pump and probe pulses at the magic angle as they cross in a 1 mm path length flowing cuvette. During photolysis, a peristaltic pump circulated the solution.

Oxygen photoconsumption. The kinetics of oxygen photoconsumption were obtained using EPR oximetry to measure changes in the oxygen concentration of irradiated samples at various times (22). Solutions of pheomelanin (1 mg mL^{-1} and 2 mg mL^{-1}) were irradiated using a 150 W compact-arc, high-pressure, xenon lamp equipped with interference filters (10 nm FWHM) to select the desired wavelength. Sample irradiance was measured with a Model IL 1400 A, International Light calibrated radiometer. Under these conditions, irradiance at the surface of the samples was less than 15 W/m^2.

RESULTS

Figures 1 and 2 show experimental FEL-PEEM data for the eumelanosomes and pheomelanosomes isolated from human hair (16). In our previous report on these pigments, a simplified Fowler equation was used to analyze the data to give threshold energies of 4.6 ± 0.2 and 3.9 ± 0.2 eV, respectively, for eumelanosomes and pheomelanosomes. The curves shown through the data points in Figs. 1 and 2 are the results of nonlinear least-squares fits of (Eq. 3) to the experimental measurements. Although the eumelanosome data can be described by a single threshold potential, the pheomelanosome data requires two threshold values to describe the wavelength-dependent signals. Both pigments exhibit a threshold

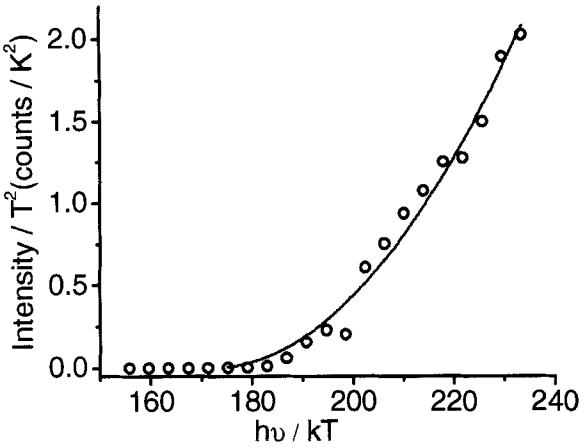

Figure 1. The integrated brightness of the PEEM image for black hair melanosomes divided by the square of the sample temperature, S/T^2, is plotted as a function of the excitation energy ($h\nu/k_BT$). The solid line is the best fit of (Eq. 3) to the data points, yielding an ionization threshold of ~4.4 ± 0.2 eV (282 nm).

of 4.4 ± 0.2 eV (282 nm). Pheomelanosomes exhibit a second threshold potential of 3.8 ± 0.2 eV (326 nm). Although these values are close to that reported earlier, using the simplified Fowler equation to describe the data masked the fact that the pheomelanosomes show two thresholds.

We have previously reported the transient absorption spectrum following excitation of solubalized synthetic pheomelanin at 350 nm (14). The transient spectrum was compared to that of the solvated electron, from which it was concluded that if excitation at this wavelength did not result in photoionization of the pigment, then the quantum yield must be less than 2×10^{-5}. In Fig. 3, we compare the transient absorption following excitation of pheomelanin at 303 nm with that of the solvated electron (23). For this excitation wavelength, there is excellent agreement between the transient spectrum of pheomelanin and that of the solvated electron. For the experimental conditions used in these measurements, the quantum yield for formation of the solvated electron is $\sim 10^{-4}$.

Table 1 presents the results of EPR oximetry measurements of the wavelength-dependent rate of oxygen uptake by synthetic pheomelanin. Data were collected for melanin concentrations of 1 and 2 mg mL^{-1}. The uptake rate scales linearly with melanin concentration. The normalized rate reported in the table is the measured uptake rate divided by the number of photons incident on the sample normalized to the experimental value for 404 nm excitation. The data show a clear increase in oxygen uptake between 338 and 323 nm.

DISCUSSION

Chedekel and coworkers reported an action spectrum for the photoconsumption of oxygen in 1980 and found that it differed significantly from the absorption spectrum of the pigment (11). Their data is reproduced in Fig. 4. The mechanism for the photoconsumption of oxygen was attributed to photoionization of the pigment followed by scavenging of the solvated electrons by molecular oxygen (Eqs. 1 and 2). These workers reported a quantum yield for this process of $\sim 7.1 \times 10^{-4}$ for excitation at 360 nm. Our analysis of the femtosecond transient spectroscopy following 350 nm excitation of solubalized pheomelanin indicated a quantum yield of less than 2×10^{-5} (22). Although the quantum yield for the photodissociation of pheomelanin is not known,

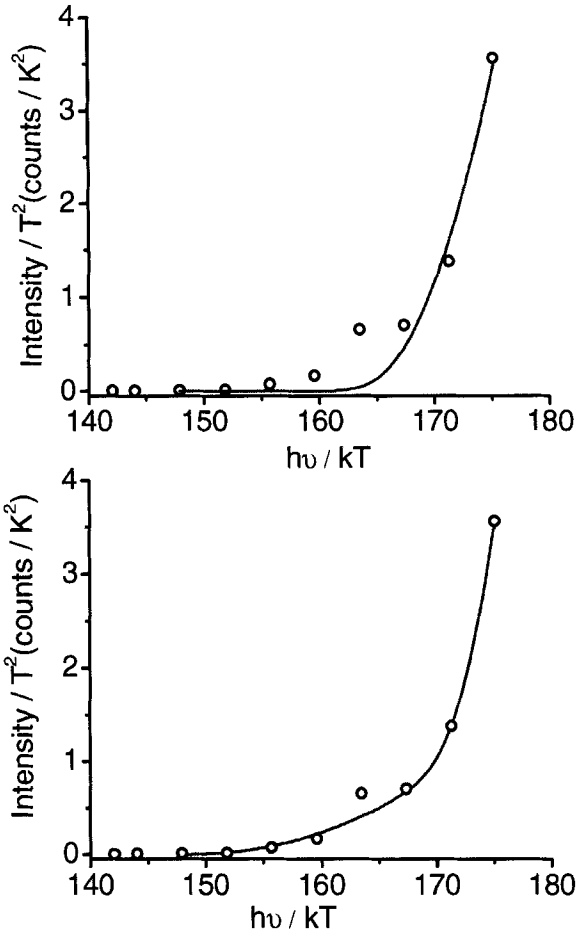

Figure 2. The integrated brightness of the PEEM image for red hair melanosomes divided by the square of the sample temperature, S/T^2, is plotted as a function of the excitation energy ($h\nu/k_BT$). Top: The solid line is the best fit of the experimental data to a single-threshold value using (Eq. 3). Bottom: The solid line is the best fit obtained for a two-threshold model where each is described by (Eq. 3). This yielded ionization thresholds of ~4.4 ± 0.2 and 3.8 ± 0.2 eV (282 and 326 nm).

benzothiazole model compounds generate e_{aq}^- with an efficiency of ~0.06, two orders of magnitude greater than the photoconsumption yields (24). Chemical analysis of synthetic melanins indicates significant chemical variation depending on preparation methods. The pigment used in our studies followed the protocols established by Ito and coworkers in 1989 (18). These protocols were published subsequent to the study by Chedekel and coworkers.

The synthetic pheomelanin used in the present study exhibited appreciable oxygen consumption in the absence of excitation. Although the change in photoconsumption uptake rate observed between 338 nm and 323 nm is reproducible, it is possible and even likely that the uptake observed for $\lambda > 338$ nm has an appreciable "dark" component. Chedekel and coworkers reported that no superoxide was observed in the absence of light, and therefore no dark reaction is taken into account in the presentation of their data. But our results on the synthetic pigments argue to the contrary. If we then consider that the constant rate of superoxide formation in the region of $\lambda > 400$ nm reflects a dark reaction, then as indicated by the dashed line in Fig. 4, the photoconsumption becomes appreciable when $\lambda < 330$, consistent with the wavelength-dependent photoconsumption data presented herein.

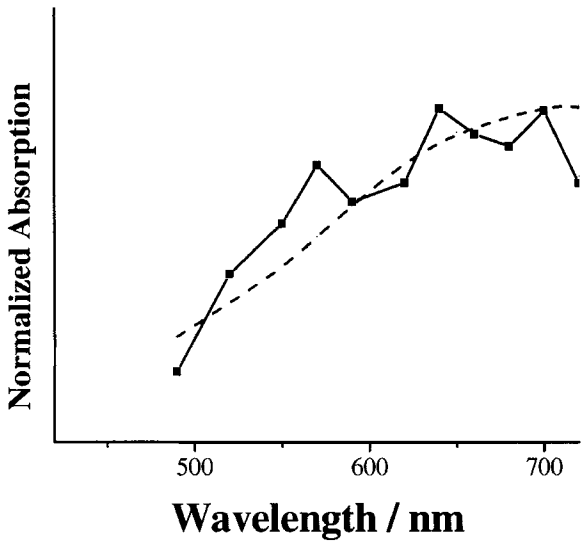

Figure 3. The transient absorption spectrum obtained 100 ps following photolysis of synthetic pheomelanin at 303 nm in water is compared to that of the solvated electron (23). The quantum yield for formation of the solvated electron is $\sim 10^{-4}$. Excellent agreement is observed. In contrast, for photolysis at 350 nm (14), no spectral evidence of solvated electron formation was detected.

Superimposed on the data of Chedekel *et al.* shown in Fig. 4 are the results from the three techniques used in the present study. FEL-PEEM indicates the lowest threshold energy for photoionization of human pheomelanosomes is 3.8 ± 0.2 eV (326 nm). The femtosecond transient spectroscopy indicates the threshold for the synthetic pigment lies between 350 nm and 303 nm. The ESR oxygen photoconsumption experiments indicate the threshold for the synthetic pigment lies between 338 nm and 323 nm. There is remarkable consistency between these data, and good agreement between the synthetic materials used in this study and the human sample.

Photoionization and photohomolysis induced by UVC irradiation was also observed in the case of synthetic pheomelanins and their precursors (25). However, unlike dopa, cysteinyldopas undergo more extensive photodecomposition, producing the carbon-centered alanyl radical. Interestingly, the photoformation of carbon-centered radical from cysteinyldopas was observed even at the longest UV-B wavelengths. Although the photochemical properties of cysteinyldopas may have important implications for cells producing these pheomelanin precursors (carbon-centered radicals have previously been shown to nick DNA), it must be stressed that no carbon-centered radicals have been observed when pheomelanin was photolyzed either with UV-C or UV-B.

Now consider the comparison of these data to the corresponding eumelanins and eumelanosomes. FEL-PEEM data indicate eumelanosomes have a threshold potential of 4.4 ± 0.2 eV (282 nm). A similar threshold is observed for the pheomelanosomes. This result is not surprising because the chemical analysis of the pheomelanosomes indicates the presence of eumelanin degradation products (16). Thus it is reasonable to conclude that the red pigment contains molecular motifs identical to eumelanin, and that these species are responsible for the higher threshold potential of the pheomelanosomes.

Using EPR-spin trapping, Kalynaraman *et al.* previously showed that irradiation of eumelanins with UV-C and UV-B results in generation of e_{aq}^- and hydrogen atoms (26). Femtosecond absorption studies of *Sepia* eumelanin do not reveal any signatures

Table 1. Wavelength-dependent rate of oxygen uptake by synthetic pheomelanin as measured by EPR oximetry. Data were collected for a melanin concentration of 2 mg mL^{-1}. The normalized rate is the measured uptake rate divided by the number of photons incident on the sample normalized to the value measured for 404 nm excitation. The last column contains the corresponding data for a melanin concentration of 1 mg mL^{-1} (run at selected wavelengths). The normalized rates are independent of the melanin concentration but the uptake rate scales linearly with melanin concentration

λ/nm	Irradiation Wm^{-2}	Uptake rate $mM\ s^{-1}$	Normalized uptake rate	Normalized uptake rate*
312	3.61	8.79×10^{-5}	3.2	—
323	4.02	9.87×10^{-5}	3.3	3.4
338	12.2	1.17×10^{-4}	1.2	—
348	7.88	1.14×10^{-4}	1.7	1.8
362	5.80	6.14×10^{-5}	1.2	—
370	7.86	1.34×10^{-4}	1.9	—
382	11.06	1.04×10^{-4}	1.0	1.1
404	15.6	1.55×10^{-5}	1.0	1.0†

*Melanin concentration of 1 mg mL^{-1}.
†Irradiation: 14.33 Wm^{-2}; uptake rate 7.04×10^{-5} $mM\ s^{-1}$.

for solvated electrons for excitation wavelengths ≥303 nm (20,27). Oxygen photoconsumption experiments do not reveal any increase in uptake rates in the region between 300 and 400 nm (20,28,29). In total, unlike pheomelanin, there is no evidence for photoionization of eumelanin in the UV-A region (λ > 320 nm).

It is of interest to examine these results in relation to the solar radiation impinging on the surface of the earth. Figure 5 shows the solar irradiance at the earth's surface for several different solar zenith angles (30). The threshold ionization energies of the human hair melanosomes obtained from FEL-PEEM are also indicated. These data clearly show that one is exposed to the wavelengths of light needed to ionization pheomelanosomes, but that the atmosphere

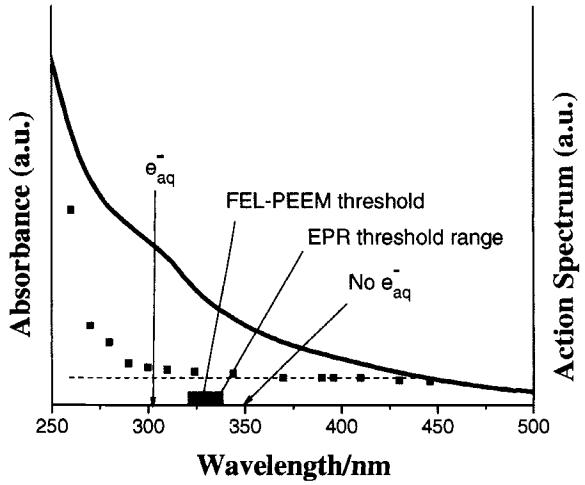

Figure 4. The absorption (solid line) and action spectrum (squares) reported by Chedekel and coworkers for the photogeneration of superoxide radical anion by synthetic pheomelanin is reproduced. Also indicated on the plot are the thresholds for photoionization determined by FEL-PEEM measurements on human pheomelanosomes, femtosecond absorption spectroscopic detection of solvated electrons, and EPR-oximetry on synthetic pigment. The constant rate of superoxide formation in the region of λ > 400 nm seen in the action spectrum is attributed to a dark reaction, and as indicated by the dashed line, the photoconsumption becomes appreciable when λ < 330. Thus, all measurements present a consistent view that the photoionization threshold of pheomelanin is around ~325 nm.

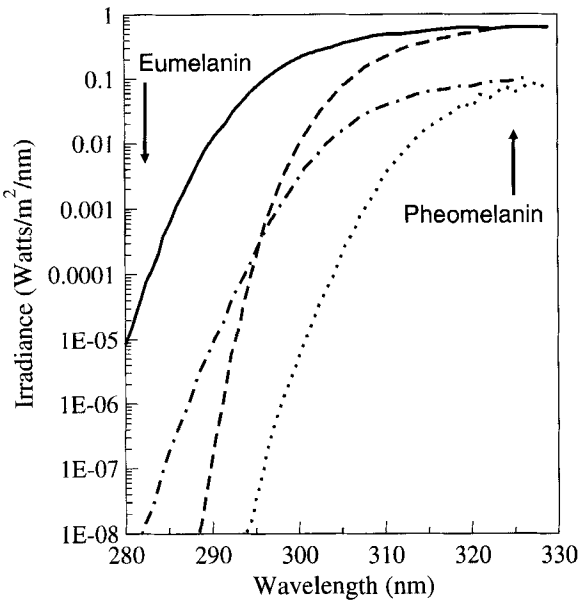

Figure 5. The incident solar radiation at the surface of the earth is plotted as a function of wavelength, solar zenith angles (SZA), and ozone concentration (in Dobson units, DU). The four curves correspond to (——) SZA = 0, 100 DU; (- - - -) SZA = 0, 400 DU; (- • - • - •) SZA = 75, 100 DU; (• • • • •) SZA = 75, 400 DU. The data were adapted from reference 30. Also indicated on the graph are the threshold ionization potentials for human eumelanosomes and pheomelanosomes. The mapping of the ionization thresholds on the solar spectrum suggests an increased photoreactivity of pheomelanosomes under normal solar exposure.

effectively (and nearly totally) blocks the energies required to photoionize eumelanosomes. In relation to previous reports indicating that pheomelanin can photosensitize cellular damage (9), the photothreshold potentials reported herein suggest that UV-induced ionization of pheomelanin is a likely candidate for the initial mechanistic step in these responses. These results collectively suggest that the photoionization of pheomelanin by UV-A radiation should be considered as a contributing source to the greater incidence rate of skin cancer in red-haired (and blond) individuals.

Acknowledgements—This work is supported by the AFOSR through the MFEL program. We thank Duke University for initial support of this work. A.P. and T.S. would like to thank the National Institutes of Health (grant RO1 EY013722) and the Polish Ministry of Science and Information Technology for providing financial support.

REFERENCES

1. Davis, T. W., F. P. Treasure, A. A. Welch and N. E. Day (2002) Epidemiology and health services research: diet and basal cell skin cancer: results from the EPIC-Norfolk cohort. *Brit. J. Dermatol.* **146**, 1017–1022.
2. Veierød, B. M., E. Weiderpass, M. Thorn, J. Hansson, E. Lund, B. Armstrong and H.-O. Adami (2003) A prospective study of pigmentation, sun exposuer and risk of cutaneous malignant melanoma in women. *J. Nat. Cancer Inst.* **95**, 1530–1538.
3. Wakamatsu, K. and S. Ito (2002) Advanced chemical methods in melanin determination. *Pigm. Cell Res.* **15**, 174–183.
4. Ito, S. (1998) Advances in chemical analysis of melanins. In *The Pigmentary System* (Edited by J. J. Nordlund, V. J. Hearing, R. A. King and J. P. Ortonne), pp. 439–450. Oxford University Press, New York.
5. Rees, J. L. (2003) Genetics of hair and skin color. *Annu. Rev. Genet.* **37**, 67–90.
6. Thody, A. J., E. M. Higgins, K. Wakamatsu, S. Ito, S. A. Burchill and J. M. Marks (1991) Pheomelanin as well as eumelanin is present in human epidermis. *J. Invest. Dermatol.* **97**(2), 340–344.
7. Vincensi, M. R., M. d'Ischia, A. Napolitano, E. M. Procaccini, G. Riccio, G. Monfrecola, P. Santoianni and G. Prota. (1998) Phaeomelanin versus eumelanin as a chemical indicator of ultraviolet sensitivity in fair-skinned subjects at high risk for melanoma: a pilot study. *Melanoma Res.* **8**, 53–58.
8. Hennessy, A., C. Oh, B. Diffey, K. Wakamatsu, S. Ito and J. Rees (2005) Eumelanin and pheomelanin concentration in human epidermis before and after UVB irradiation. *Pigm. Cell Res.* **18**, 220–223.
9. Wenczl, E., G. P. Van der Schans, L. Roza, R. M. Kolb, A. J. Timmerman, N. P. M. Smit, S. Pavel and A. A. Schothorst. (1998) (Pheo)melanin photosensitizes UVA-induced DNA damage in cultured human melanocytes. *J. Invest. Dermatol.* **111**, 678–682.
10. Takeuchi, S., W. Zhang, K. Wakamatsu, S. Ito, V. J. Hearing, K. H. Kraemer and D. E. Brash (2004) Melanin acts as a potent UVB photosensitizer to cause an atypical mode of cell death in murine skin. *Proc. Natl. Acad. Sci.* **101**, 15076–15081.
11. Chedekel, M. R., P. P. Agin and R. M. Sayre. (1980) Photochemistry of pheomelanin—action spectrum for superoxide production. *Photochem. Photobiol.* **31**, 553–555.
12. Chedekel, M. R., S. K. Smith, P. W. Post, A. Pokora and D. L. Vessell (1978) Photodestruction of pheomelanin: role of oxygen. *Proc. Natl. Acad. Sci.* **75**, 5395–5399.
13. Chedekel, M. R., P. W. Post, R. M. Deibel and M. Kalus (1977) Photodestruction of phaeomelanin. *Photochem. Photobiol.* **26**, 651–653.
14. Ye, T. and J. D. Simon (2002) Ultrafast spectroscopic study of pheomelanin: implications on the mechanism of superoxide anion formation. *J. Phys. Chem. B* **106**, 6133–6135.
15. Samokhvalov, A., J. Garguilo, W.-C. Yang, G. S. Edwards, R. J. Nemanich and J. D. Simon (2004) Photoionization threshold of eumelanosomes determined using UV free electron laser–photoelectron emission microscopy. *J. Phys. Chem. B* **108**, 16334–16338.
16. Samokhvalov, A., L. Hong, Y. Liu, J. Garguilo, R. J. Nemanich, G. S. Edwards and J. D. Simon (2005) Oxidation potentials of human eumelanosomes and pheomelanosomes. *Photochem. Photobio.* **81**, 145–148.
17. Liu, Y., L. Hong, C. R. Bowers, K. Wakamatsu, S. Ito and John D. Simon (2005) Comparison of the structural, chemical, and spectroscopic properties of human black and red hair melanosomes. *Photochem. Photobio.* **81**, 135–144.
18. Liu, Y. and J. D. Simon (2003) Isolation and biophysical studies of natural eumelanins: applications of imaging technologies and ultrafast spectroscopy. *Pigm. Cell Res.* **16**, 606–618.
19. Ito, S. (1989) Optimization of conditions for preparing synthetic pheomelanin. *Pigm. Cell. Res.* **2**, 53–56.
20. Fowler, R. H. (1931) The analysis of photoelectric sensitivity curves for clean metals at various temperatures. *Phys. Rev.* **38**, 45–56.
21. Ye, T. and J. D. Simon (2003) Comparison of the ultrafast absorption dynamics of eumelanin and pheomelanin. *J. Phys. Chem. B* **107**, 11240–11244.
22. Sarna, T. and R. C. Sealy (1984) Photoinduced oxygen consumption in melanin systems—action spectra and quantum yields for eumelanin and synthetic melanin. *Photochem. Photobiol.* **39**, 69–74.
23. Hart, E. J. and M. Anbar (1970) *The Hydrated Electron.* John Wiley & Sons, Inc., San Diego.
24. Lambert, C., R. S. Sinclair, T. G. Truscott, E. J. Land, M. R. Chedekel and C.-T. Liu (1984) Photochemistry of benzothiazole models of pheomelanin. *Photochem. Photobiol.* **39**, 5–10.
25. Pilas, B., C. C. Felix, T. Sarna and B. Kalyanaraman (1986) Photolysis of pheomelanin precursors: an ESR-spin trapping study. *Photochem. Photobiol.* **44**, 689–696.
26. Kalyanaraman, B., C. C. Felix and R. C. Sealy (1984) Photoionization and photohomolysis of melanins: an electron spin resonance-spin trapping study. *J. Am. Chem. Soc.* **106**, 7327–7330.
27. Nofsinger, J. B., T. Ye and J. D. Simon (2001) Ultrafast nonradiative relaxation dynamics of eumelanin. *J. Phys. Chem. B* **105**, 2864–2866.
28. Sarna, T., I. A. Menon and R. C. Sealy (1985) Photosensitization of melanins—a comparative study. *Photochem. Photobiol.* **42**, 529–532.
29. Sarna, T. and R. C. Sealy (1984) Free radicals from eumelanins—quantum yields and wavelength dependence. *Arch. Biochem. Biophys.* **232**, 574–578.
30. Gibson, J. H. UVB radiation: definition and characteristics. Available at: http://uvb.nrel.colostate.edu/UVB/publications/uvb_primer.pdf, accessed 3 January 2006.